Geophysical Research Letters

RESEARCH LETTER
10.1029/2024GL108825

Precipitation Control on Weathering Intensity and Depositional Flux of Meteoric ^{10}Be Revealed From Soil Profiles Along a Climate Gradient (Chile)

Laura V. Krone[1,2], Hella Wittmann[2], and Friedhelm von Blanckenburg[1,2]

[1]Institute of Geological Sciences, Freie Universität Berlin, Berlin, Germany, [2]GFZ German Research Centre for Geosciences, Potsdam, Germany

Key Points:

- The ratio of meteoric cosmogenic ^{10}Be to stable ^{9}Be was used to determine soil denudation rates
- In regolith profiles, both the infiltration depth of ^{10}Be and the fraction of ^{9}Be released by weathering depends on precipitation
- Atmospheric models reflect the flux of meteoric ^{10}Be well in humid areas; in arid areas the flux strongly depends on local precipitation

Correspondence to:

L. V. Krone,
l.krone@fu-berlin.de

Citation:

Krone, L. V., Wittmann, H., & von Blanckenburg, F. (2024). Precipitation control on weathering intensity and depositional flux of meteoric ^{10}Be revealed from soil profiles along a climate gradient (Chile). *Geophysical Research Letters*, *51*, e2024GL108825. https://doi.org/10.1029/2024GL108825

Received 26 FEB 2024
Accepted 24 JUL 2024

Abstract Along a climate gradient in the Chilean coastal mountains, we investigated denudation rates using the meteoric cosmogenic nuclide ^{10}Be and its ratio to stable ^{9}Be, and chemical depletion fractions (CDFs) in bulk soil samples. We find that the fraction of ^{9}Be released from bedrock is a sensitive indicator of weathering, similar to CDF. Meteoric ^{10}Be decreases exponentially with depth, reflecting the reactive nature of this tracer. We also measured denudation rates by the well-understood in situ cosmogenic ^{10}Be system on quartz. Assuming that both systems record the same denudation rate we calculated the depositional flux of meteoric ^{10}Be for each study site. The flux agrees to that derived from atmospheric models in the mediterranean and humid areas. In contrast, in the arid and semi-arid areas, the calculated flux agrees with a precipitation-derived flux, indicating delivery of ^{10}Be to be affected by small-scale climatic variations not reflected by current atmospheric models.

Plain Language Summary To identify how geologic and climatic conditions control how fast soil is removed from the Earth's surface (denudation), we need to measure these rates over long periods, like thousands of years. A common method makes use of a rare radioactive nuclide, cosmogenic ^{10}Be, formed by cosmic rays in quartz. However, if rocks do not contain quartz, an alternative system is provided by meteoric cosmogenic ^{10}Be precipitated from the atmosphere and stable ^{9}Be that is released during rock weathering. From the ratio ^{10}Be to ^{9}Be we can estimate denudation rates if we know the fraction of ^{9}Be released by weathering and how much meteoric ^{10}Be is deposited from the atmosphere per unit time and area. In a comparison with the quartz-based method we explored these two unknowns on soil samples from four locations in Chile with different climates, all from granitic rock. We discovered two key points: (a) The amount of stable ^{9}Be indicates soil alteration, which depends on water infiltration. (b) In arid climate, the deposition of meteoric ^{10}Be is limited by rainfall, whereas in areas of sufficient yearly rainfall the ^{10}Be deposition reflects large-scale atmospheric distribution and is predicted by combined global cosmogenic nuclide production and climate models.

1. Introduction

The depth of the weathering zone, fluid flow through this zone, and removal of primary and secondary minerals by erosion all represent interdependent controls over rock weathering and soil formation. The ^{10}Be(meteoric)/^{9}Be cosmogenic isotope system is an underexplored proxy in depth profiles capable to track all of these controls (von Blanckenburg et al., 2012). Application of this proxy to determine basin-wide denudation rates in river samples yielded denudation rates (D_{met}) that are in good agreement with rates determined by the well-studied in situ cosmogenic ^{10}Be system (D_{insitu}; e.g. Portenga et al., 2019; Wittmann et al., 2015). Here, we apply meteoric ^{10}Be/^{9}Be to depth profiles in soil to evaluate the method's suitability for determining D_{met} from single soil samples in the Chilean Coastal Cordillera. We further estimate the meteoric ^{10}Be depositional flux, an essential prerequisite for the application of meteoric ^{10}Be, by assuming that both systems record the same denudation rate such that the "unknown" meteoric ^{10}Be depositional flux can be calculated.

Meteoric ^{10}Be (^{10}Be$_{met}$), with a half-life of 1.39 Myr (Chmeleff et al., 2010), is produced in the atmosphere predominantly by cosmic ray-induced spallation, attaches to atmospheric aerosols and is delivered to Earth's surface by wet and dry deposition (Lal & Peters, 1967; Willenbring & von Blanckenburg, 2010). After deposition, it is incorporated into amorphous and weakly crystalline (Mn-Fe-Al)-oxides, -hydroxides, -oxyhydroxides, clay or organic phases (Barg et al., 1997; Willenbring & von Blanckenburg, 2010). Such so-called reactive (reac) phases can be extracted from soils or sediments via sequential extraction. The ^{10}Be fraction retained in the solid depends on pH and grain size. Normalization of the ^{10}Be concentration in the reactive phase to stable ^{9}Be

concentration resulting from the release from rock during weathering (reactive $^{9}Be_{reac}$ and dissolved $^{9}Be_{diss}$) largely removes this dependence (Wittmann et al., 2012). The resulting isotope ratio of meteoric ^{10}Be to ^{9}Be ($^{10}Be_{met}/^{9}Be_{reac}$) is a proxy for weathering and denudation (von Blanckenburg et al., 2012). Compared to $^{10}Be_{insitu}$, which is produced in the mineral lattice of for example, quartz predominantly by cosmic-ray induced spallation (Lal, 1991), $^{10}Be_{met}$ is present in higher concentrations, can be applied to quartz-free lithologies like mafic rock (Dannhaus et al., 2018) or slate (Deng, Yang, et al., 2020), and requires much smaller sample amounts.

To apply $^{10}Be_{met}/^{9}Be_{reac}$, three parameters need to be known: The first is the concentration of stable ^{9}Be in unweathered bedrock (denoted as $[^{9}Be]_{parent}$). The second is the fraction of ^{9}Be released from weathering ($f^{9}Be_{reac} + f^{9}Be_{diss}$). This fraction quantifies the mobilization of ^{9}Be from primary minerals, comprising ^{9}Be precipitated or adsorbed onto reactive mineral surfaces ($f^{9}Be_{reac}$) or lost into the dissolved phase ($f^{9}Be_{diss}$). These fractions can be determined from the ratio of the concentration of ^{9}Be in reactive phases ($[^{9}Be]_{reac}$) such as (Mn-Fe-Al)-oxides, clay or organic phases to the concentration of ^{9}Be in the mineral-bound phase ($[^{9}Be]_{min}$; von Blanckenburg et al., 2012), provided that dissolved loss of ^{9}Be is negligible which is the case if pH is high or runoff is low. The third is the depositional flux (F_{met}^{10Be}) of $^{10}Be_{met}$ to Earth's surface. The production of ^{10}Be in the atmosphere depends on air pressure, and varies with geomagnetic field intensity and solar activity (Masarik & Beer, 1999, 2009). $^{10}Be_{met}$ is well-mixed in the stratosphere and therefore latitudinal production variations are averaged out (Heikkilä et al., 2013). Within a residence time of ∼1 year, $^{10}Be_{met}$ attaches to atmospheric aerosol particles and is delivered to Earth's surface (McHargue & Damon, 1991). F_{met}^{10Be} constitutes three distinct pathways that depend on atmospheric properties: ^{10}Be by precipitation as wet delivery, by dry delivery on aerosol particles, and by dust which is, however, recycled ^{10}Be (Deng, Wittmann, et al., 2020). Some studies suggest that the depositional flux correlates with precipitation (Field et al., 2006; Graly et al., 2011; Heikkilä & Smith, 2013; Heikkilä et al., 2013). Other studies noted dilution of $^{10}Be_{met}$ with higher precipitation (e.g., Yiou et al., 1997). These two effects, the "additive" and the "dilution" effect, are explored in detail in Willenbring and von Blanckenburg, (2010) and Deng, Wittmann, et al. (2020). Mostly, these effects operate in combination, where their relative weight depends on the ratio of the area of vapor condensation to the area of precipitation (Deng, Wittmann, et al., 2020).

A variety of approaches is used to estimate F_{met}^{10Be}: (a) general circulation models (GCM) combined with ^{10}Be production functions and aerosol dynamics; (b) ^{10}Be in precipitation collections; (c) ^{10}Be inventories in dated soil profiles; (d) riverine ^{10}Be exported by solids and in the dissolved form (summarized in Deng, Wittmann, et al., 2020). GCMs provide F_{met}^{10Be} on a large spatial scale (Heikkilä & von Blanckenburg, 2015) while precipitation collection provides local short-term fluxes influenced by seasonal variations and stratosphere-troposphere exchange of air masses (Graly et al., 2011). Deng, Wittmann, et al. (2020) found that precipitation-derived F_{met}^{10Be} mostly exceed GCM-derived fluxes. Therefore, F_{met}^{10Be} estimated with the empirical equation by Graly et al. (2011) based on precipitation-collections might overestimate long-term deposition where precipitation is high. F_{met}^{10Be} from soil profile measurements and GCMs are generally lower than those from precipitation collections which can be attributed to potential incomplete sampling of rainfall samples or loss by erosion in soils. However, all flux agree within a factor of 2 (Deng, Wittmann, et al., 2020).

Here we explored the precipitation dependence of $^{10}Be_{met}$ deposition and identified possible limitations of the $^{10}Be_{met}/^{9}Be_{reac}$ denudation rate meter by comparing D_{insitu} and D_{met} on eroding soil profiles, an approach previously employed only once (Clow et al., 2020). The principle is based on assuming that $D_{insitu} = D_{met}$ so that F_{met}^{10Be} can be calculated from known D_{insitu}. To do so we measured $^{10}Be_{insitu}$, the inventory of $^{10}Be_{met}$, $^{9}Be_{parent}$, $^{9}Be_{reac}$, and $^{9}Be_{min}$ concentrations in soil and drill core samples, and calculated denudation, erosion, and weathering rates, as well as F_{met}^{10Be}. By employing this method along a climate gradient in the Chilean Coastal Cordillera we show that weathering intensity depends on precipitation, and therefore on the accumulation and mobilization of Be in depth profiles. We also show that in arid areas F_{met}^{10Be} depends on local precipitation, while in humid areas F_{met}^{10Be} is reflected by atmospheric models.

2. Study Sites and Previous Work

The study sites Pan de Azúcar (PdA), Santa Gracia (SG), La Campana (LC), and Nahuelbuta (NA) are located along a climate gradient between 26°S and 38°S in the Chilean Coastal Cordillera that was studied by the research

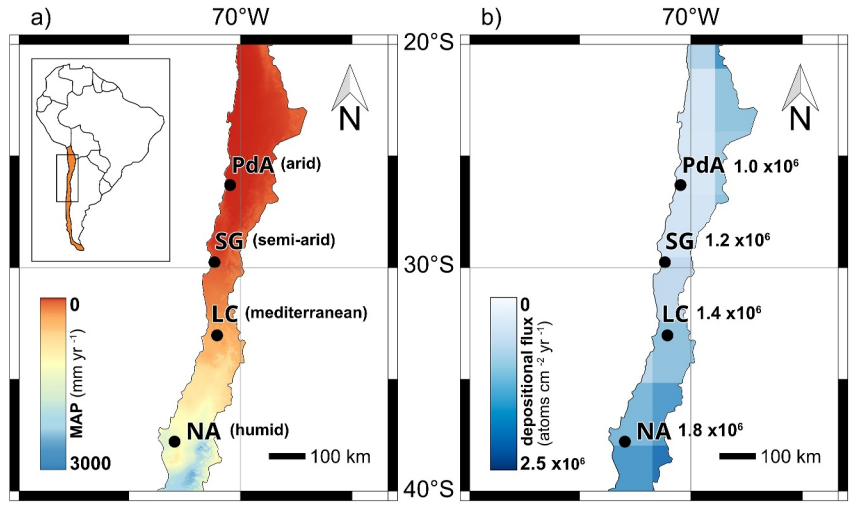

Figure 1. Sampling locations in Chile. (a) Mean annual precipitation averaged from 1970 to 2000 (Fick & Hijmans, 2017: worldclim.org). (b) Meteoric ^{10}Be depositional flux map from production functions implemented in the ECHAM5-HAM general circulation models model (Heikkilä, 2007; Heikkilä & von Blanckenburg, 2015) which also shows the cell size of model values of 200 × 200 km.

program "Earthshape" (Figure 1). This gradient covers arid (PdA, 10 mm yr^{-1} average precipitation rate), semi-arid (SG, 90 mm yr^{-1}), mediterranean (LC, 440 mm yr^{-1}), and humid (NA, 1,100 mm yr^{-1}) climate with vegetation cover ranging from <5% in arid to 100% in humid climate (Oeser et al., 2018a). The lithology consists of granodiorites, tonalites and quartz diorites (Oeser et al., 2018a; SERNAGEOMIN, 2003). Hydrothermal alteration of the granite is strong at the arid study site, and weak at the semi-arid site as apparent by a high degree of Fe-oxidation and fracture fillings by both carbonates and amorphous Fe-oxides (Hampl et al., 2022; Krone et al., 2021a). A detailed geologic description is available in Oeser et al. (2018a) and Krone et al. (2021a). Previous studies also report on soil-pit-derived (Schaller et al., 2018) and river-sediment-derived (van Dongen et al., 2019) D_{insitu}. The soil-pit derived D_{insitu} were on average 9.6 ± 1.4, 19.2 ± 3.1, 61 ± 8, and 33 ± 15 t km^{-2} yr^{-1} from arid to humid climate.

3. Materials and Methods

We sampled the upper 2–6 m of soil profiles at all sites and used visually unweathered parent rock from bedrock drill core samples from >10 m below the weathering front recovered during wireline diamond drilling campaigns (March 2019–March 2020; Krone et al., 2021a). The depth profiles are located on topographic ridges (semi-arid, mediterranean, humid-NA1) and at the foot of a slope (arid, humid-NA2).

The detailed procedure for in situ and meteoric ^{10}Be analyses is provided in Krone et al. (2024). To determine denudation rates D_{insitu}, we used the CRONUS online exposure age calculator (Balco et al., 2008) using the time-dependent scaling scheme of Lal/Stone (St) (Lal, 1991; Stone, 2000) and a sea-level high latitude neutron spallation ^{10}Be production rate of 4.01 at g^{-1} yr^{-1} (Borchers et al., 2016). D_{insitu} (g cm^{-2} yr^{-1}) can be calculated using Equation 1 shown in a simplified form (Lal, 1991):

$$D_{insitu} = \left(\frac{P}{[^{10}Be_{insitu}]} - \lambda \right) * \Lambda \quad (1)$$

where $[^{10}Be_{insitu}]$ is the ^{10}Be nuclide concentration (atoms g_{qtz}^{-1}), P the scaled ^{10}Be production rate (atoms g_{qtz}^{-1} yr^{-1}), and λ the ^{10}Be decay constant (5×10^{-7} yr^{-1}). Λ includes the e-folding absorption length for neutrons and muons, respectively.

Denudation rates D_{met} (g cm^{-2} yr^{-1}) were calculated using equation 12 from von Blanckenburg et al. (2012) solved for D_{met} with an additional term to account for decay of meteoric reactive ^{10}Be (hereafter $^{10}Be_{reac}$) that may reduce the soil inventory if the infiltration depth is deep and denudation rate is slow:

$$D_{\text{met}} = \frac{F_{\text{met}}^{^{10}\text{Be}} - I * \lambda}{\left(\frac{^{10}\text{Be}}{^{9}\text{Be}}\right)_{\text{reac}} * \left[^{9}\text{Be}\right]_{\text{parent}} * \left(f^{9}\text{Be}_{\text{reac}} + f^{9}\text{Be}_{\text{diss}}\right)} \quad (2)$$

with $F_{\text{met}}^{^{10}\text{Be}}$ as meteoric ^{10}Be depositional flux (atoms cm^{-2} yr^{-1}), ^{9}Be concentrations ([^{9}Be], atoms g^{-1}) for the reac and min fractions, and parent bedrock, respectively, I as the $^{10}\text{Be}_{\text{reac}}$ inventory of the soil profile (atoms cm^{-2}) and λ as decay constant of ^{10}Be (yr^{-1}). We calculated $F_{\text{met}}^{^{10}\text{Be}}$ by solving Equation 2 for $F_{\text{met}}^{^{10}\text{Be}}$ assuming that $D_{\text{insitu}} = D_{\text{met}}$. $f^{9}\text{Be}_{\text{reac}} + f^{9}\text{Be}_{\text{diss}}$ is calculated from $[^{9}\text{Be}]_{\text{reac}}$ and $[^{9}\text{Be}]_{\text{min}}$, assuming negligible or minor (humid) dissolved loss of ^{9}Be:

$$f^{9}\text{Be}_{\text{reac}} + f^{9}\text{Be}_{\text{diss}} = \frac{\left[^{9}\text{Be}\right]_{\text{reac}}}{\left(\left[^{9}\text{Be}\right]_{\text{min}} + \left[^{9}\text{Be}\right]_{\text{reac}}\right)} \quad (3)$$

To derive the weathering rate W from a denudation rate D, we use the chemical depletion fraction (CDF):

$$\text{CDF} = 1 - \frac{[X_i]_{\text{bedrock}}}{[X_i]_{\text{weathered}}} \quad (4)$$

with $[X_i]_{\text{bedrock}}$ and $[X_i]_{\text{weathered}}$ as the concentration of an immobile element (PdA, LC, NA: Nb; SG: Zr) in bedrock and weathered material. The weathering rate $W_{\text{met or insitu}}$ is calculated using the mean CDF (Table 1; Krone et al., 2021b) from surface samples according to Equation 4.

$$W_{\text{met or insitu}} = D_{\text{met or insitu}} * \text{CDF} \quad (5)$$

The erosion rate E_{insitu} can be calculated from D_{insitu} and W_{insitu}.

$$E_{\text{insitu}} = D_{\text{insitu}} - W_{\text{insitu}}. \quad (6)$$

4. Results

We provide all results in a data publication (Tables S1–S5, Krone et al., 2024); main results are listed in Table 1. Blank ^{10}Be/^{9}Be ratios are $3.4 \pm 0.8 \times 10^{-15}$ and $6.5 \pm 5.7 \times 10^{-15}$ for in situ and meteoric ^{10}Be, respectively. Denudation rates from $^{10}\text{Be}_{\text{insitu}}$ are 7.1 ± 0.5 t km^{-2} yr^{-1} at the arid (uncertainty is the standard deviation of 3 measured D_{insitu}), 29.6 ± 4.0 t km^{-2} yr^{-1} at the semi-arid (Krone et al., 2021a), 126 ± 32 t km^{-2} yr^{-1} at the mediterranean, and 38 ± 10 t km^{-2} yr^{-1} at the humid site. The new D_{insitu} from our soil samples are in good agreement with published in situ denudation rates (Schaller et al., 2018; van Dongen et al., 2019).

$[^{9}\text{Be}]_{\text{parent}}$ is 1.9 ± 0.5 µg g^{-1} at the arid, 1.2 ± 0.1 µg g^{-1} at the semi-arid, 1.0 ± 0.1 µg g^{-1} at the mediterranean, and 1.4 ± 0.4 to 2.1 ± 0.1 µg g^{-1} at the humid site (relative uncertainty 5%). These concentrations are at the lower end of 3.1 ± 1.5 µg g^{-1} $[^{9}\text{Be}]_{\text{parent}}$ compiled for granitoid lithology (von Blanckenburg et al., 2012). $f^{9}\text{Be}_{\text{reac}} + f^{9}\text{Be}_{\text{diss}}$ is highest with 0.46 at the arid site and lowest at the semi-arid and mediterranean sites with 0.11 and 0.12, respectively, and 0.26 at the humid site (Figure 2b). $[^{9}\text{Be}]_{\text{reac}}$ shows no gradient with depth. $[^{10}\text{Be}]_{\text{met}}$ in topsoil samples correlates with precipitation by showing an increasing concentration from the arid ($1.2 \pm 0.21 \times 10^{7}$ atoms g^{-1}) to the humid ($4.5 \pm 0.15 \times 10^{8}$ atoms g^{-1}) site (Figure 2c). In the depth profiles, reactive $[^{10}\text{Be}]_{\text{reac}}$ decreases exponentially from surface to depth at all study sites (Figure 2c).

For the calculation of D_{met}, we used the GCM model-derived $F_{\text{met}}^{^{10}\text{Be}}$ by Heikkilä and von Blanckenburg (2015) for the respective sites (Table 1). At the mediterranean and humid sites, D_{met} are 169 ± 39 and 30 ± 8 t km^{-2} yr^{-1}, respectively. D_{met} for the arid site is 1,235 ± 460 and for the semi-arid site 210 ± 22 t km^{-2} yr^{-1}. These latter two rates disagree strongly with D_{insitu}. We discuss the reasons below and do not consider these two D_{met} as meaningful estimates any further.

Geophysical Research Letters

10.1029/2024GL108825

Table 1
Main Results for All Study Sites

								In situ ^{10}Be		Meteoric ^{10}Be/^{9}Be	
	$F^{10}Be_{met}$ (GCM-derived) (atoms cm^{-2} yr^{-1})	$F^{10}Be_{met}$ (from Graly et al. (2011)) (atoms cm^{-2} yr^{-1})	$F^{10}Be_{met}$ (this study) (atoms cm^{-2} yr^{-1})	(^{10}Be/^{9}Be) ($\times10^{-9}$ atoms $atoms^{-1}$)	$[^{9}Be]_{parent}$ ($\times10^{17}$ atoms g^{-1})	$f\,^{9}Be_{reac} + f\,^{9}Be_{min}$	CDF	D (t km^{-2} yr^{-1})	E (t km^{-2} yr^{-1})	D (GCM-derived F) (t km^{-2} yr^{-1})	D (precipitation-derived F) (t km^{-2} yr^{-1})
PdA	$1.0 \pm 0.2 \times 10^{6}$	$1.5 \pm 0.3 \times 10^{4}$	$6.3 \pm 2.0 \times 10^{3}$	0.14 ± 0.03	1.2 ± 0.4	0.46	0.00 ± 0.00	7.1 ± 0.5	7.1 ± 0.5	$(1{,}235 \pm 460)$[a]	18 ± 7
SG	$1.2 \pm 0.01 \times 10^{6}$	$1.7 \pm 0.3 \times 10^{5}$	$1.6 \pm 0.3 \times 10^{5}$	6.4 ± 0.4	0.81 ± 0.05	0.11	0.33 ± 0.02	30 ± 4	19.7 ± 2.7	(210 ± 22)[a]	30 ± 7
LC	$1.4 \pm 0.3 \times 10^{6}$	$1.0 \pm 0.2 \times 10^{6}$	$1.1 \pm 0.3 \times 10^{6}$	11.3 ± 0.7	0.65 ± 0.03	0.12	0.21 ± 0.05	126 ± 32	99 ± 25	169 ± 39	119 ± 27
NA1 Ridge	$1.8 \pm 0.4 \times 10^{6}$	$3.0 \pm 0.6 \times 10^{6}$	$1.1 \pm 0.3 \times 10^{6}$	19 ± 1	0.95 ± 0.26	0.25	0.50 ± 0.06	24 ± 1	11.9 ± 2.4	40 ± 14	65 ± 23
NA2 Slope	$1.8 \pm 0.4 \times 10^{6}$	$3.0 \pm 0.6 \times 10^{6}$	$3.3 \pm 0.3 \times 10^{6}$	19 ± 1	1.4 ± 0.05	0.27	0.56 ± 0.02	45 ± 2	19.8 ± 2.6	24 ± 5	40 ± 9
NA_{avg}	$1.8 \pm 0.4 \times 10^{6}$	$3.0 \pm 0.6 \times 10^{6}$	$2.2 \pm 0.7 \times 10^{6}$	19 ± 1	1.2 ± 0.2	0.26	0.53 ± 0.02	38 ± 10	17.5 ± 3.9	30 ± 8	50 ± 13

Note. CDF: chemical depletion fraction; $F^{10}Be_{met}$: depositional flux; D: total denudation rate; E: physical erosion rate. [a]These denudation and erosion rates are overestimated because of flux deficits (see Section 5).

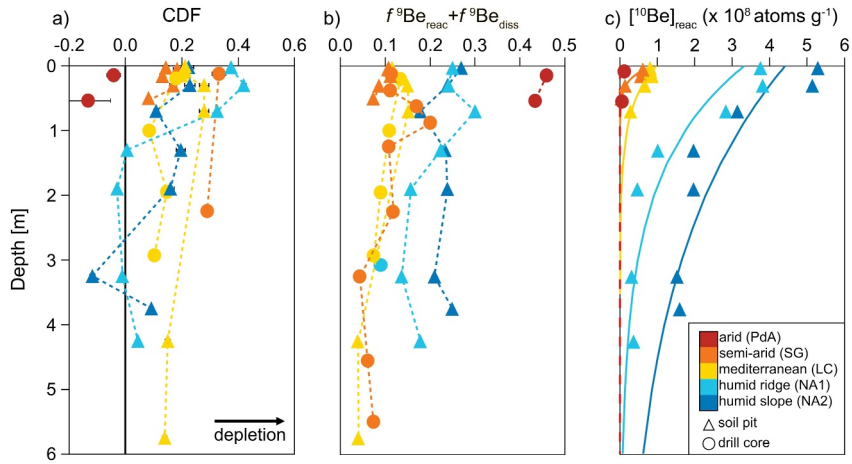

Figure 2. (a) Chemical depletion fraction (CDF), black line indicates zero depletion, positive values indicate depletion. Used immobile element: Nb for arid, mediterranean, humid, Zr for semi-arid. Uncertainties are calculated from bedrock variability of Zr or Nb. Data for semi-arid site from Krone et al. (2021b). (b) $f^{9}Be_{reac} + f^{9}Be_{diss}$ as indicator for the degree of ^{9}Be mobilization from primary mineral and retention in the reactive phase with depth (zero values denote no mobilization, unity denotes quantitative transfer from primary to reactive phases). (c) meteoric $[^{10}Be]_{reac}$ with depth (dashed line indicates detection limit of 9.3×10^{5} atoms g^{-1}, solid lines show exponential fits used to calculate ^{10}Be inventories). Symbol sizes exceed the size of most uncertainty bars. These are provided in Table 1.

By inserting D_{insitu} in Equation 2 and solving for $F_{met}^{^{10}Be}$, we obtain $F_{met}^{^{10}Be}$ values covering three orders of magnitude of $(6.3 \pm 2.0) \times 10^{3}$ at the arid, $(1.6 \pm 0.3) \times 10^{5}$ at the semi-arid, $(1.1 \pm 0.3) \times 10^{6}$ at the mediterranean, and $(1.1 \pm 0.3$ to $3.3 \pm 0.3) \times 10^{6}$ atoms cm^{-2} yr^{-1} at the humid site.

5. Discussion

5.1. Weathering Proxies From Surface Soil and Soil Profiles

The humid sites reveal highest $f^{9}Be_{reac} + f^{9}Be_{diss}$ and CDF along the gradient (where the arid site provides an outlier discussed below; Figure 2a). At the humid site precipitation is highest which leads to highest degree of bulk element loss (indicated by CDF) and of ^{9}Be mobilization from bedrock into the reactive phase ($f^{9}Be_{reac} + f^{9}Be_{diss}$). At the mediterranean and semi-arid sites $f^{9}Be_{reac} + f^{9}Be_{diss}$ are similar; yet the CDF indicates higher loss at the semi-arid site. There, the high abundance of soluble plagioclase results in a high weatherability of bedrock as indicated by CDF and mobilization of ^{9}Be even with limited water availability (Table S3 in Oeser et al., 2018b). Both water flow and mineral assemblage of bedrock are therefore controls over the degree of weathering, indicated by both CDF and $f^{9}Be_{reac} + f^{9}Be_{diss}$. Compared to the CDF, ^{9}Be mobilization as quantified by $f^{9}Be_{reac} + f^{9}Be_{diss}$ offers a practical advantage as it does not require knowing the concentration of an insoluble index element in both regolith and bedrock. The Be-specific weathering degree $f^{9}Be_{reac} + f^{9}Be_{diss}$ can be determined on a single soil sample.

The highest $f^{9}Be_{reac} + f^{9}Be_{diss}$ was found at the arid site. This alteration cannot be due to weathering given the lack of water flow. At this site, chemical mass loss by weathering as quantified by CDF is not detectable, and geophysical subsurface imaging does not reveal a weathered zone at the top of the profile. However, fractured bedrock is imaged from the surface to approx. 20 m depth (Trichandi et al., 2024). Along these fractures parent rock is strongly hydrothermally overprinted. This hydrothermal activity likely mobilized ^{9}Be (Barton & Young, 2002), rendering $f^{9}Be_{reac} + f^{9}Be_{diss}$ an indicator for hydrothermalism rather than for weathering at this site. Potentially a mild hydrothermal overprint at the semi-arid site might have also caused ^{9}Be mobilization (Krone et al., 2021a).

For meteoric $[^{10}Be]_{reac}$ in soil profiles, "decline-type" profiles emerge if Be movement to depth is retarded (Graly et al., 2010; Maher & von Blanckenburg, 2016; Willenbring & von Blanckenburg, 2010) and regolith mixing with depth is absent (McKean et al., 1993). We identified decline-type profiles with exponential decrease of $[^{10}Be]_{reac}$

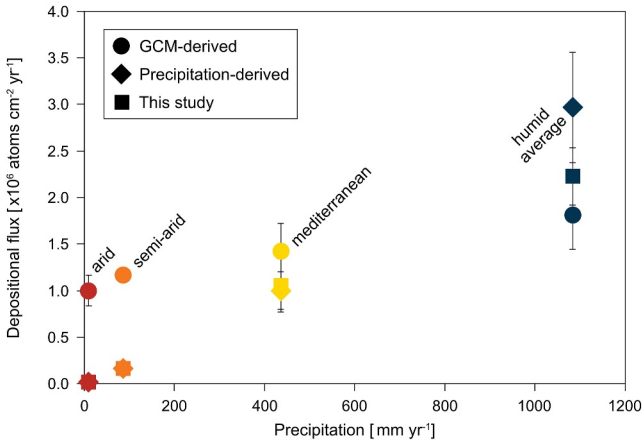

Figure 3. Depositional flux for $^{10}Be_{met}$ derived from general circulation models (Heikkilä & von Blanckenburg, 2015), precipitation (Graly et al., 2011), and from combined D_{insitu} and $^{10}Be_{met}$ in soil surface samples (this study).

attaining a zero value in approx. 1 m (semi-arid), approx. 2.5 m (mediterranean) and approx. 6–12 m (humid; Figure 2c) depth. At the arid site, we cannot identify this depth due to the low sample size ($n = 2$). The infiltration depth is correlated with the amount of precipitation. This observation corresponds to a model that predicts deeper infiltration depths at higher flow rates (Maher & von Blanckenburg, 2016).

The infiltration depth is deepest at the humid site with 5 m, despite the high abundance of clay minerals in the uppermost profile meter (Hampl et al., 2023) that are thought to adsorb ^{10}Be. Deeper in the profile clay minerals are less abundant (approx. 5%–10%; Hampl et al., 2023) and scale with the declining concentration of ^{10}Be. Three independent controls over adsorption and infiltration of ^{10}Be likely favor the deep infiltration, as predicted by reactive flow models of Maher and von Blanckenburg, (2016): First, at the humid site fluid flow is highest, second, soil pH is lowest (4–5 at the humid site compared to 6–7 at the mediterranean site and 7–8 at the other sites), and third, the residence time of a given length interval of regolith (and thus the time available for depth migration) as calculated from denudation rates (see below) is about three times as long at the humid site than at the mediterranean site.

5.2. Denudation Rates and ^{10}Be Depositional Flux Estimates

Denudation rates calculated from $^{10}Be_{met}/^{9}Be_{reac}$ and GCM-derived F_{met}^{10Be} indicate a dependence regarding the topographic position where the sample was taken from. At the humid site, we observe that the sample from the ridge position (NA1) yields higher D_{met} (40 t km^{-2} yr^{-1}) than D_{insitu} (24 t km^{-2} yr^{-1}) and vice versa at the slope position (NA2; D_{met} is 25 t km^{-2} yr^{-1} and D_{insitu} is 45 t km^{-2} yr^{-1}; Table 1). Where runoff is high, downslope transport of surface-derived fine soil particles rich in $^{10}Be_{met}$ might cause loss of $^{10}Be_{met}$ at the ridge and its accumulation on the slope (Schoonejans et al., 2017).

The calculated D_{met} agree within uncertainty with D_{insitu} at the mediterranean and humid sites (Figure 3, Table S5, Krone et al., 2024). In contrast, they strongly disagree at the semi-arid and arid sites (Table 1). The disagreement is most pronounced at the arid site, where the calculated D_{met} exceeds D_{insitu} ~170-fold. The cause of this disagreement is an overestimation of F_{met}^{10Be} from the atmospheric model at these dry sites. This finding becomes apparent when D_{met} is equated with D_{insitu} to estimate F_{met}^{10Be} (Equation 2, Table 1). At the arid sites, the derived F_{met}^{10Be} is only 5,700 atoms cm^{-2} yr^{-1} which is ~2 orders of magnitude lower than GCM-derived F_{met}^{10Be} (Heikkilä & von Blanckenburg, 2015). Using the same principle, the precipitation-derived flux (Graly et al., 2011) closely matches the F_{met}^{10Be} estimated from equating denudation rates at the arid and semi-arid sites. At the humid site, the precipitation-derived flux exceeds the model-derived F_{met}^{10Be} by about 30%. At the mediterranean site, fluxes from all three methods agree within uncertainty.

We consider the lack of precipitation as the main cause for the observed deficit in $^{10}Be_{met}$ deposition at the dry sites. A similar observation was made in a previous study from the Atacama Desert, where F_{met}^{10Be} of $(3.7 \pm 0.6) \times 10^4$ atoms cm^{-2} yr^{-1} was estimated, which is only 6% of the corresponding GCM-model flux for this region (Wang et al., 2015). Taken together, while these two studies for the first time quantify the low depositional ^{10}Be fluxes in arid areas, they also offer two consistent explanations for the GCM-derived F_{met}^{10Be} overestimating $^{10}Be_{met}$ deposition in dry regions. First, although in the model the fraction of dry deposition in total ^{10}Be deposition is 0.2–0.4 in this region (Heikkilä et al., 2013), dry deposition does not appear to be a significant delivery mechanism. Second, fine-scale spatial variations of aridity in the Atacama Desert are not adequately represented by the coarse resolution of the GCM-model with a cell size of approx. 200 × 200 km.

The arid and semi-arid sites are subjected to occasional influx of moisture in the form of coastal fog that, however, does not cause $^{10}Be_{met}$ deposition. In this region, the coastal fog is transported from the Pacific Ocean toward the Coastal Cordillera (Lehnert et al., 2018). If the travel distance is sufficiently long, the additive effect operates on ^{10}Be, meaning the fog accumulates ^{10}Be scavenged from the atmosphere (Deng, Wittmann, et al., 2020).

Deuterium/hydrogen isotope ratios (in δ^2H, seawater ratio = 0) measured on the land surface indicate the travel distance of precipitation as the isotopes fractionate during rainfall (Araguás-Araguás et al., 2000). Near the coast, a ratio of −34‰ ± 5‰ indicates a proximal moisture source (arid site; Bowen, 2023), while further inland the δ^2H ratio decreases to approx. −70‰ to −90‰ in the Andes as heavy isotopes are preferentially lost during precipitation (Araguás-Araguás et al., 2000). We can therefore exclude coastal fog as a main supplier of $^{10}Be_{met}$ in the arid site. Comparing the arid and semi-arid to the mediterranean and humid sites, convective precipitation appears to be the relevant deposition mechanism for $^{10}Be_{met}$ at the latter sites. At these sites of convective precipitation, the atmospheric models appear to provide representative estimates of $F_{met}^{10_{Be}}$. In contrast, at the dry sites a precipitation-driven model appears to approach actual fluxes more accurately than coarse-resolution atmospheric models.

6. Implications

Both Be isotopes are sensitive indicators of the controls over weathering in the critical zone, albeit in different ways: Meteoric ^{10}Be indicates the depth extent of infiltration of particle-reactive elements, as controlled by fluid flow, reactive surfaces, pH, and soil residence time. The fraction of ^{9}Be released from primary minerals, in contrast, serves as a sensitive indicator of regolith alteration, either from hydrothermal overprinting as is the case at our arid site, or from meteoric water-induced weathering, as at the sites exposed to higher rainfall. At these latter sites, this fraction is a sensitive indicator of the weathering degree.

Our findings suggest that at sites of predominantly convective precipitation GCM-derived estimates of $F_{met}^{10_{Be}}$ are representative. Therefore, in such climate of sufficient precipitation these models are suited as input for denudation rate determination with meteoric ^{10}Be. In aris and semi-arid areas and high variability in precipitation over short distances, $F_{met}^{10_{Be}}$ from coarse-resolution atmospheric transport models fail to resolve these gradients, and also appear to overestimate dry deposition of ^{10}Be. In these climatic settings, the precipitation-derived $F_{met}^{10_{Be}}$ is better-suited to derive denudation rates, given its better resolution of spatially variable rainfall. Resolving these dependencies in detail across different methods will be a useful research avenue for future applications of the $^{10}Be/^{9}Be$ system. To this end, comparing D_{insitu} and D_{met} at a given eroding setting as employed here appears to hold promise. Moreover, on hillslopes the role of downslope transport affecting $[^{10}Be]_{met}$ requires further investigation for applying the isotope ratio as a denudation rate meter at different topographic positions.

Our comparison with D_{insitu} shows that when knowing $F_{met}^{10_{Be}}$, ^{9}Be concentration of local bedrock, and mobilization of ^{9}Be by weathering, reliable denudation rates result from $^{10}Be_{met}/^{9}Be_{reac}$. In that case a single sample from surface soil is sufficient to determine a local denudation rate.

Conflict of Interest

The authors declare no conflicts of interest relevant to this study.

Data Availability Statement

The dataset is available under Krone et al. (2024): The depositional flux of meteoric ^{10}Be derived from combined in situ and meteoric ^{10}Be analyses along a climate gradient (Chile). GFZ Data Services. https://doi.org/10.5880/fidgeo.2024.021.

Acknowledgments
This project is funded by German Science Foundation (DFG)-Grant BL562-16/2 within the priority program 1803 "EarthShape—Earth surface shaping by biota." We are grateful to the "DeepEarthshape"-team for assistance during the drilling campaigns. Open Access funding enabled and organized by Projekt DEAL.

References

Araguás-Araguás, L., Froehlich, K., & Rozanski, K. (2000). Deuterium and oxygen-18 isotope composition of precipitation and atmospheric moisture. *Hydrological Processes*, *14*(8), 1341–1355. https://doi.org/10.1002/1099-1085(20000615)14:8<1341::AID-HYP983>3.0.CO;2-Z

Balco, G., Stone, J. O., Lifton, N. A., & Dunai, T. J. (2008). A complete and easily accessible means of calculating surface exposure ages or erosion rates from ^{10}Be and ^{26}Al measurements. *Quaternary Geochronology*, *3*(3), 174–195. https://doi.org/10.1016/j.quageo.2007.12.001

Barg, E., Lal, D., Pavich, M. J., Caffee, M. W., & Southon, J. R. (1997). Beryllium geochemistry in soils: Evaluation of $^{10}Be/^{9}Be$ ratios in authigenic minerals as a basis for age models. *Chemical Geology*, *140*(3–4), 237–258. https://doi.org/10.1016/S0009-2541(97)00051-X

Barton, M. D., & Young, S. (2002). Non-pegmatitic deposits of beryllium: Mineralogy, geology, phase equilibria and origin. *Reviews in Mineralogy and Geochemistry*, *50*(1), 591–691. https://doi.org/10.2138/rmg.2002.50.14

Borchers, B., Marrero, S., Balco, G., Caffee, M., Goehring, B., Lifton, N., et al. (2016). Geological calibration of spallation production rates in the CRONUS-Earth project. *Quaternary Geochronology*, *31*, 188–198. https://doi.org/10.1016/j.quageo.2015.01.009

Bowen, G. J. (2023). The online isotopes in precipitation calculator, version 3.2. Retrieved from http://www.waterisotopes.org

Chmeleff, J., Von Blanckenburg, F., Kossert, K., & Jakob, D. (2010). Determination of the ^{10}Be half-life by multicollector ICP-MS and liquid scintillation counting. *Nuclear Instruments and Methods in Physics Research Section B: Beam Interactions with Materials and Atoms*, *268*(2), 192–199. https://doi.org/10.1016/j.nimb.2009.09.012

Clow, T., Willenbring, J. K., Schaller, M., Blum, J. D., Christl, M., Kubik, P. W., & Von Blanckenburg, F. (2020). Calibrating a long-term meteoric ^{10}Be delivery rate into eroding western US glacial deposits by comparing meteoric and in situ produced ^{10}Be depth profiles. *Geochronology*, *2*(2), 411–423. https://doi.org/10.5194/gchron-2-411-2020

Dannhaus, N., Wittmann, H., Krám, P., Christl, M., & von Blanckenburg, F. (2018). Catchment-wide weathering and erosion rates of mafic, ultramafic, and granitic rock from cosmogenic meteoric ^{10}Be/^{9}Be ratios. *Geochimica et Cosmochimica Acta*, *222*, 618–641. https://doi.org/10.1016/j.gca.2017.11.005

Deng, K., Wittmann, H., & von Blanckenburg, F. (2020). The depositional flux of meteoric cosmogenic ^{10}Be from modeling and observation. *Earth and Planetary Science Letters*, *550*, 116530. https://doi.org/10.1016/j.epsl.2020.116530

Deng, K., Yang, S., Von Blanckenburg, F., & Wittmann, H. (2020). Denudation rate changes along a fast-eroding mountainous river with slate headwaters in Taiwan from ^{10}Be (Meteoric)/^{9}Be ratios. *Journal of Geophysical Research: Earth Surface*, *125*(2), e2019JF005251. https://doi.org/10.1029/2019JF005251

Fick, S. E., & Hijmans, R. J. (2017). WorldClim 2: New 1-km spatial resolution climate surfaces for global land areas. *International Journal of Climatology*, *37*(12), 4302–4315. https://doi.org/10.1002/joc.5086

Field, C. V., Schmidt, G. A., Koch, D., & Salyk, C. (2006). Modeling production and climate-related impacts on ^{10}Be concentration in ice cores. *Journal of Geophysical Research*, *111*(D15), D15107. https://doi.org/10.1029/2005JD006410

Graly, J. A., Bierman, P. R., Reusser, L. J., & Pavich, M. J. (2010). Meteoric ^{10}Be in soil profiles—A global meta-analysis. *Geochimica et Cosmochimica Acta*, *74*(23), 6814–6829. https://doi.org/10.1016/j.gca.2010.08.036

Graly, J. A., Reusser, L. J., & Bierman, P. R. (2011). Short and long-term delivery rates of meteoric ^{10}Be to terrestrial soils. *Earth and Planetary Science Letters*, *302*(3–4), 329–336. https://doi.org/10.1016/j.epsl.2010.12.020

Hampl, F. J., Schiperski, F., Byrne, J. M., Schwerdhelm, C., Kappler, A., Bryce, C., et al. (2022). The role of iron-bearing minerals for the deep weathering of a hydrothermally altered plutonic rock in semi-arid climate (Chilean Coastal Cordillera). *Chemical Geology*, *604*, 120922. https://doi.org/10.1016/j.chemgeo.2022.120922

Hampl, F. J., Schiperski, F., Schwerdhelm, C., Stroncik, N., Bryce, C., von Blanckenburg, F., & Neumann, T. (2023). Feedbacks between the formation of secondary minerals and the infiltration of fluids into the regolith of granitic rocks in different climatic zones (Chilean Coastal Cordillera). *Earth Surface Dynamics*, *11*(3), 511–528. https://doi.org/10.5194/esurf-11-511-2023

Heikkilä, U. (2007). *Modeling of the atmospheric transport of the cosmogenic radionuclides ^{10}Be and ^{7}Be using the ECHAM5-HAM general circulation model*. ETH Zurich. https://doi.org/10.3929/ETHZ-A-005560259

Heikkilä, U., Beer, J., Abreu, J. A., & Steinhilber, F. (2013). On the atmospheric transport and deposition of the cosmogenic Radionuclides (^{10}Be): A review. *Space Science Reviews*, *176*(1–4), 321–332. https://doi.org/10.1007/s11214-011-9838-0

Heikkilä, U., & Smith, A. M. (2013). Production rate and climate influences on the variability of ^{10}Be deposition simulated by ECHAM5-HAM: Globally, in Greenland, and in Antarctica: Production and climate influence on ^{10}BE. *Journal of Geophysical Research: Atmospheres*, *118*(6), 2506–2520. https://doi.org/10.1002/jgrd.50217

Heikkilä, U., & von Blanckenburg, F. (2015). The global distribution of Holocene meteoric ^{10}Be fluxes from atmospheric models. Distribution maps for terrestrial Earths surface applications [Dataset]. *GFZ Data Services*. https://doi.org/10.5880/GFZ.3.4.2015.001

Krone, L. V., Hampl, F. J., Schwerdhelm, C., Bryce, C., Ganzert, L., Kitte, A., et al. (2021a). Deep weathering in the semi-arid coastal Cordillera, Chile. *Scientific Reports*, *11*(1), 13057. https://doi.org/10.1038/s41598-021-90267-7

Krone, L. V., Hampl, F. J., Schwerdhelm, C., Bryce, C., Ganzert, L., Kitte, A., et al. (2021b). Physical and geochemical data on a drill core from the semi-arid Coastal Cordillera, Chile [Dataset]. *GFZ Data Services*. https://doi.org/10.5880/GFZ.3.3.2021.002

Krone, L. V., Wittmann, H., & von Blanckenburg, F. (2024). The depositional flux of meteoric ^{10}Be derived from combined in situ and meteoric ^{10}Be analyses along a climate gradient (Chile) [Dataset]. *GFZ Data Services*. https://doi.org/10.5880/fidgeo.2024.021

Lal, D. (1991). Cosmic ray labeling of erosion surfaces: In situ nuclide production rates and erosion models. *Earth and Planetary Science Letters*, *104*(2–4), 424–439. https://doi.org/10.1016/0012-821X(91)90220-C

Lal, D., & Peters, B. (1967). Cosmic ray produced radioactivity on the Earth. In K. Sitte (Ed.), *Kosmische Strahlung II/cosmic rays II* (Vol. 9/46/2, pp. 551–612). Springer. https://doi.org/10.1007/978-3-642-46079-1_7

Lehnert, L. W., Thies, B., Trachte, K., Achilles, S., Osses, P., Baumann, K., et al. (2018). A case study on fog/low Stratus occurrence at Las Lomitas, Atacama Desert (Chile) as a water source for biological soil crusts. *Aerosol and Air Quality Research*, *18*(1), 254–326. https://doi.org/10.4209/aaqr.2017.01.0021

Maher, K., & von Blanckenburg, F. (2016). Surface ages and weathering rates from ^{10}Be (meteoric) and ^{10}Be/^{9}Be: Insights from differential mass balance and reactive transport modeling. *Chemical Geology*, *446*, 70–86. https://doi.org/10.1016/j.chemgeo.2016.07.016

Masarik, J., & Beer, J. (1999). Simulation of particle fluxes and cosmogenic nuclide production in the Earth's atmosphere. *Journal of Geophysical Research*, *104*(D10), 12099–12111. https://doi.org/10.1029/1998JD200091

Masarik, J., & Beer, J. (2009). An updated simulation of particle fluxes and cosmogenic nuclide production in the Earth's atmosphere. *Journal of Geophysical Research*, *114*(D11), D11103. https://doi.org/10.1029/2008JD010557

McHargue, L. R., & Damon, P. E. (1991). The global beryllium 10 cycle. *Reviews of Geophysics*, *29*(2), 141–158. https://doi.org/10.1029/91RG00072

McKean, J. A., Dietrich, W. E., Finkel, R. C., Southon, J. R., & Caffee, M. W. (1993). Quantification of soil production and downslope creep rates from cosmogenic ^{10}Be accumulations on a hillslope profile. *Geology*, *21*(4), 343. https://doi.org/10.1130/0091-7613(1993)021<0343:QOSPAD>2.3.CO;2

Oeser, R. A., Stroncik, N., Moskwa, L.-M., Bernhard, N., Schaller, M., Canessa, R., et al. (2018a). Chemistry and microbiology of the Critical Zone along a steep climate and vegetation gradient in the Chilean Coastal Cordillera. *Catena*, *170*, 183–203. https://doi.org/10.1016/j.catena.2018.06.002

Oeser, R. A., Stroncik, N., Moskwa, L.-M., Bernhard, N., Schaller, M., Canessa, R., et al. (2018b). Data supplement to: Chemistry and microbiology of the critical zone along a steep climate and vegetation gradient in the Chilean coastal Cordillera [Dataset]. *GFZ Data Services*. https://doi.org/10.5880/GFZ.3.3.2018.001

Portenga, E. W., Bierman, P. R., Trodick, C. D., Greene, S. E., DeJong, B. D., Rood, D. H., & Pavich, M. J. (2019). Erosion rates and sediment flux within the Potomac River basin quantified over millennial timescales using beryllium isotopes. *GSA Bulletin*, *131*(7–8), 1295–1311. https://doi.org/10.1130/B31840.1

Schaller, M., Ehlers, T. A., Lang, K. A. H., Schmid, M., & Fuentes-Espoz, J. P. (2018). Addressing the contribution of climate and vegetation cover on hillslope denudation, Chilean Coastal Cordillera (26°–38°S). *Earth and Planetary Science Letters*, *489*, 111–122. https://doi.org/10.1016/j.epsl.2018.02.026

Schoonejans, J., Vanacker, V., Opfergelt, S., & Christl, M. (2017). Long-term soil erosion derived from in-situ ^{10}Be and inventories of meteoric ^{10}Be in deeply weathered soils in southern Brazil. *Chemical Geology*, *466*, 380–388. https://doi.org/10.1016/j.chemgeo.2017.06.025

SERNAGEOMIN. (2003). Mapa Geológico de Chile: Versión digital, No. 4 CD-R, versión 1. In *Servicio Nacional de Geología y Minería, Publicación Geológica Digital, No. 4 CD-R, versión 1*.

Stone, J. O. (2000). Air pressure and cosmogenic isotope production. *Journal of Geophysical Research*, *105*(B10), 23753–23759. https://doi.org/10.1029/2000JB900181

Trichandi, R., Bauer, K., Ryberg, T., Heit, B., Araya Vargas, J., Von Blanckenburg, F., & Krawczyk, C. M. (2024). 3D shear wave velocity imaging of the subsurface structure of granite rocks in the arid climate of Pan de Azúcar, Chile, revealed by Bayesian inversion of HVSR curves. *Earth Surface Dynamics*, *12*(3), 747–763. https://doi.org/10.5194/esurf-12-747-2024

van Dongen, R., Scherler, D., Wittmann, H., & von Blanckenburg, F. (2019). Cosmogenic ^{10}Be in river sediment: Where grain size matters and why. *Earth Surface Dynamics*, *7*(2), 393–410. https://doi.org/10.5194/esurf-7-393-2019

von Blanckenburg, F., Bouchez, J., & Wittmann, H. (2012). Earth surface erosion and weathering from the ^{10}Be (meteoric)/^{9}Be ratio. *Earth and Planetary Science Letters*, *351–352*, 295–305. https://doi.org/10.1016/j.epsl.2012.07.022

Wang, F., Michalski, G., Seo, J.-H., Granger, D. E., Lifton, N., & Caffee, M. (2015). Beryllium-10 concentrations in the hyper-arid soils in the Atacama Desert, Chile: Implications for arid soil formation rates and El Niño driven changes in Pliocene precipitation. *Geochimica et Cosmochimica Acta*, *160*, 227–242. https://doi.org/10.1016/j.gca.2015.03.008

Willenbring, J. K., & von Blanckenburg, F. (2010). Meteoric cosmogenic Beryllium-10 adsorbed to river sediment and soil: Applications for Earth-surface dynamics. *Earth-Science Reviews*, *98*(1–2), 105–122. https://doi.org/10.1016/j.earscirev.2009.10.008

Wittmann, H., von Blanckenburg, F., Bouchez, J., Dannhaus, N., Naumann, R., Christl, M., & Gaillardet, J. (2012). The dependence of meteoric ^{10}Be concentrations on particle size in Amazon River bed sediment and the extraction of reactive ^{10}Be/^{9}Be ratios. *Chemical Geology*, *318–319*, 126–138. https://doi.org/10.1016/j.chemgeo.2012.04.031

Wittmann, H., von Blanckenburg, F., Dannhaus, N., Bouchez, J., Gaillardet, J., Guyot, J. L., et al. (2015). A test of the cosmogenic ^{10}Be (meteoric)/^{9}Be proxy for simultaneously determining basin-wide erosion rates, denudation rates, and the degree of weathering in the amazon basin: Erosion from meteoric ^{10}BE/^{9}BE in amazon. *Journal of Geophysical Research: Earth Surface*, *120*(12), 2498–2528. https://doi.org/10.1002/2015JF003581

Yiou, F., Raisbeck, G. M., Baumgartner, S., Beer, J., Hammer, C., Johnsen, S., et al. (1997). Beryllium 10 in the Greenland ice core project ice core at summit, Greenland. *Journal of Geophysical Research*, *102*(C12), 26783–26794. https://doi.org/10.1029/97JC01265